# Computational Estimation of Potential Inhibitors from the Known Drugs against the Main Protease of SARS-CoV-2

Nguyen Minh Tam[1,2], Minh Quan Pham[3,4], Nguyen Xuan Ha[5], Pham Cam Nam,[6] Huong Thi Thu Phung[7*]

[1] *Computational Chemistry Research Group, Ton Duc Thang University, Ho Chi Minh City, Vietnam*
[2] *Faculty of Applied Sciences, Ton Duc Thang University, Ho Chi Minh City, Vietnam*
[3]*Institute of Natural Products Chemistry, Vietnam Academy of Science and Technology, Hanoi, Vietnam*
[4]*Graduate University of Science and Technology, Vietnam Academy of Science and Technology, Hanoi, Vietnam*
[5]*Faculty of Chemistry and Environment, Thuyloi University, Ministry of Agriculture and Rural Development, Hanoi, Vietnam*
[6]*Department of Chemical Engineering, The University of Da Nang-University of Science and Technology, Da Nang City, Vietnam*
[7]*NTT Hi-Tech Institute, Nguyen Tat Thanh University, Ho Chi Minh City, Vietnam.*
**Corresponding author*
*Email: ptthuong@ntt.edu.vn*

## Abstract

The coronavirus disease (COVID-19) pandemic caused by a severe acute respiratory syndrome coronavirus 2 (SARS-CoV-2) has rapidly spread worldwide recently, leading to a global social and economic disruption. Although the emergently approved vaccine programs against SARS-CoV-2 have been rolled out globally, the number of COVID-19 daily cases and deaths has remained significantly high. Here, we attempted to computationally screen for possible medications for COVID-19 via rapidly estimate the highly potential inhibitors from an FDA-approved drug database against the main protease (Mpro) of SARS-CoV-2. The approach combined molecular docking and fast pulling of ligand (FPL) simulations that were demonstrated to be accurate and suitable for quick prediction of SARS-CoV-2 Mpro inhibitors. The results suggested that twenty-seven compounds were capable of strongly associating with SARS-CoV-2 Mpro. Among them, the seven top leads are *daclatasvir, teniposide, etoposide, levoleucovorin, naldemedine*, *cabozantinib,* and *irinotecan*. The potential application of these drugs in COVID-19 therapy has thus been discussed.

Keywords: binding free energy; fast pulling ligand; FDA-approved drugs; molecular docking; potential inhibitors; SARS-CoV-2 Mpro

## Introduction

The ongoing mortal pneumonia disease (COVID-19) caused by a severe acute respiratory syndrome coronavirus 2 (SARS-CoV-2) has unstoppably spread globally since its first identification in December 2019. In March 2020, the World Health Organization (WHO) classified the COVID-19 outbreak as "Global Pandemic" [1]. The transmission rate of the viral infection is extremely high [2] while the fatality rate ranges from 1% to 12% [3]. Recently, the COVID-19 disease has affected 221 countries and territories around the world with approximately 112 million reported cases and 2.5 million mortality [4].

SARS-CoV-2 has a single-stranded positive-sense RNA genome with a length of approximately 29.9 kb [5, 6]. The viral genome is composed of 11 open reading frames coding for more than 20 different proteins. Among them, the SARS-CoV-2 main protease (Mpro), one of the most important proteins during the viral translation, is required to digests polyproteins at eleven or more conserved cleavage sites to produce various functional proteins [7]. The polypeptides generated are critical for the viral transcription and replication during its infection. The SARS-CoV-2 Mpro is well conserved in the *Coronaviridae* family [8] while its closely related homologs in humans have lacked. These characteristics cause Mpro one of the most interesting targets for the selection of antiviral drugs to restrain the SARS-CoV-2 growth and replication [9]. Consequently, multiple investigations have been done to define the promising inhibitors of this protease [7, 10-15].

Nowadays, the computer-aided drug design (CADD) approach has been broadly shown to remarkably save time and cost in the development of a new medication [16, 17]. In CADD, the ligand-binding free energy $\Delta G$ of an inhibitor with the targeted protein can be accurately predicted via molecular dynamics (MD) simulations [16, 18]. Accordingly, rapidly and precisely estimating the ligand-binding free energy is extremely essential for identifying potential inhibitors [19-21]. Previously, the fast pulling of ligand (FPL)

simulations was shown to effectively and accurately estimate the relative binding affinities of small molecules against HIV-1 protease or CHK1 with an affordable CPU time consumption [22, 23]. It is worthy to mention that the computational combination of molecular docking and the FPL approach was validated on available inhibitors of SARS-CoV-2 Mpro and showed good agreement between calculated binding free energies and experimental values [12, 13, 24]. In this study, the possible inhibitors of SARS-CoV-2 Mpro were screened from FDA-approved drugs using a combination of molecular docking and the FPL simulations. The results revealed that twenty-seven compounds could interact with high affinity to SARS-CoV-2 Mpro. These compounds thus become potential candidates for drugs against the COVID-19 disease effectively.

## Materials and Methods

### Structure of SARS-CoV-2 Mpro and Ligands

The crystal structure of SARS-COV-2 Mpro in monomeric form (6Y2F) was downloaded from the Protein Data Bank [10]. The structure of ligands was obtained from the ZINC15 sub-database named FDA-approved drugs [25].

### Molecular Docking Simulations

The Autodock Vina version 1.1 package was utilized to dock the screened ligands to the SARS-CoV-2 Mpro [26]. The parameters of the molecular docking simulations were prepared by AutodockTools 1.5.6 [27] following the earlier studies [12, 28]. In detail, the exhaustiveness parameter of global searching that corresponds to the accuracy of the docking simulation was defined as 8 which represents default options. The atomic charges of protein and ligands were anticipated using the Gasteiger–Marsili approach [29, 30]. The protein and ligands were emblemed by a united atom model with explicit polar hydrogens [31]. The maximum energy difference between the worst and best docking modes was set to 7 kcal/mol. The grid center of Vina docking was selected as the center of mass of compound α-ketoamide **13b**, which was obtained using the experimental pose [10]. The highest binding affinity profiles were chosen as the best docking conformation. The docking grid was determined as 2.6 × 2.6 × 2.6 nm which is able to accommodate the whole targeted active site [12-14, 24].

## Molecular Dynamics Simulations

We used the GROMACS version 5.1.5 [32] to simulate the conformation change of the complex SARS-CoV-2 Mpro and ligand. The protein and ions were parameterized using the Amber99SBILDN force field [33]. The water molecules were topologized via the TIP3P water model [34]. The general Amber force field (GAFF) [35] was applied to represent the ligand using AmberTools18 [36]. Combining the AMBER99SB-ILDN force field and water model provides one of the best options to estimate the free energy [37, 38]. The restrained electrostatic potential (RESP) method [39] was used to fit the ligand atomic charges based on density functional theory (DFT) calculations using the combination of the B3LYP functional and 6-31G(d,p) basis set. The AMBER force field format was transformed to GROMACS using the ACPYPE protocol [40]. The time steps of MD simulations were set to 2 fs. MD simulations were carried out with an integrator at the absolute temperature of 300 K controlled by V-rescale. The 0.9 nm cutoff was applied to the non-bonded atoms pair list. The steepest descent method was initially applied to the complex of SARS-CoV-2 Mpro and inhibitor to minimize the system. To relax the system, the 0.1 ns of NVT and 2.0 ns of NPT simulations were computed. During the NVT and NPT ensembles, the $C_\alpha$ atoms of SARS-CoV-2 Mpro were positionally restrained by a small harmonic force of 1,000 kJ/mol/nm$^2$. The solvated complexes were recorded every 10 ps over MD simulations.

## Fast Pulling of Ligand Simulations

The last snapshot of NPT simulations was then applied as the starting conformation of the steered-MD (SMD) simulation [22]. The complex of SARS-CoV-2 and ligand was covered into a rectangular periodic boundary conditions box (9.83 × 5.92 × 8.70 nm) [12, 24, 41]. More than 50,000 atoms including SARS-CoV-2 Mpro, ligand, water molecules and counter-balanced ions $Na^+$ were involved in the simulated system. To pull the ligand out of the binding site in SARS-CoV-2 Mpro, an external harmonic force $F = k(vt - z)$ along the Z-axis was applied on the center of mass of the ligand in the complex system (a spring constant of the cantilever of $k$ = 0.005•nm•ps$^{-1}$, pulling speed of $v$ = 600 kJ•mol$^{-1}$•nm$^{-2}$, and $z$ is the displacement of the ligand mass center from its initial position) [24, 41-43]. The work of external force $W$ is calculated according to the following equation:

$$W = v \int_0^t F(t)dt \quad (1)$$

During SMD simulations, the solvated complex systems were recorded the external pulling force and the ligand displacement every 0.1 ps for the estimation of the ligand-binding affinity [22]. For better sampling, 8 non-equilibrium MD simulation trajectories were independently conducted for each ligand-Mpro complex beginning with the same initial crystal structure but different random velocities. The mean external work $\langle W \rangle$ was averaged from 8 SMD trajectories for each complex.

### Analyzed Tools

To predict the ligand protonation state, the Chemicalize tools (www.chemicalize.com), a website application of the ChemAxon, were utilized. A hydrogen bond is defined if the angle of an acceptor (A)–hydrogen (H)–donor (D) is larger than 135° with the distance from A to D is smaller than 0.35 nm. A sidechain contact is determined if the distance between non-hydrogen atoms of SARS-CoV-2 Mpro and the ligands is smaller than 0.45 nm. The interaction between the SARS-CoV-2 Mpro protein and the ligand was illustrated by LigPlot$^+$ software [44].

## Results and Discussion

### Molecular Docking Simulation

The SARS-CoV-2 Mpro in monomeric form can be used as a target for CADD to prevent the function of SARS-CoV-2 Mpro [12, 13, 24]. Autodock Vina [45], an open-source docking package, is one of the most popular docking protocols to rapidly estimate the binding affinity and binding pose of the protein and ligand complex. To validate the suitability of the approach, Autodock Vina was first applied to dock 21 SARS-CoV-2 Mpro inhibitors that have been confirmed experimentally. As was expected, the approach formed appropriate results for calculating the ligand-binding affinities of SARS-CoV-2 (Table 1) with a correlation coefficient correlation of $R_{\mathrm{Dock}}$ = 0.66 ± 0.12 (Figure 1), which is in good agreement with the recent work [41]. Additionally, the root-mean-square error (RMSE) concerning practical data was calculated as $RMSE$ = 0.83 ± 0.19 kcal mol$^{-1}$. Noted that the results reported are consistent with the earlier studies [13, 14].

**Table 1**. The binding affinity values of verified SARS-CoV-2 Mpro inhibitors obtained via the docking simulations.

| No | Inhibitor | $\Delta G_{Dock}{}^{a}$ | $\Delta G_{exp}{}^{b}$ |
|---|---|---|---|
| 1 | **11a** | -9.96 | -7.60 |
| 2 | **11b** | -10.13 | -7.20 |
| 3 | **11r** | -9.23 | -6.90 |
| 4 | **13a** | -7.70 | -6.80 |
| 5 | **13b** | -8.45 | -6.70 |
| 6 | *Carmofur* | -7.86 | -6.60 |
| 7 | *Disulfiram* | -6.89 | -6.10 |
| 8 | *Ebselen* | -8.45 | -5.70 |
| 9 | *PX-12* | -6.39 | -5.60 |
| 10 | *Shikonin* | -6.58 | -3.90 |
| 11 | *Tideglusib* | -7.95 | -3.80 |
| 12 | *Digitoxin* | -9.09 | -8.00 |
| 13 | *Oubain* | -9.6 | -7.20 |
| 14 | *Remdesivir* | -6.96 | -6.40 |
| 15 | *Oxyclozanide* | -7.44 | -6.30 |
| 16 | *Ebastine* | -7.06 | -6.10 |
| 17 | *Toremifene* | -7.46 | -5.90 |
| 18 | *Hexachlorophene* | -8.28 | -5.70 |
| 19 | *Chloroquine* | -6.74 | -5.60 |
| 20 | *Triparanol* | -7.05 | -5.50 |
| 21 | *Favipiravir* | -4.52 | -4.80 |

[a]The docking scores $\Delta G_{Dock}$ were obtained via the Autodock Vina package.

[b]The experimental binding free energy $\Delta G_{exp}$ was roughly identified using the reported values [46] of inhibition constant $IC_{50}$ with an assumption that $IC_{50}$ is equal to $k$i. The unit is in kcal $mol^{-1}$.

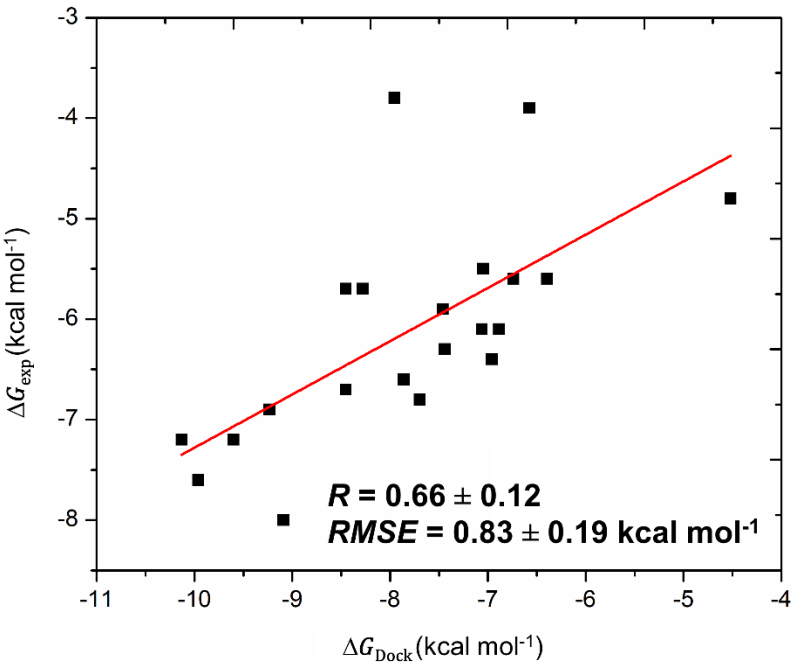


**Figure 1**. Correlation between molecular docking and experiment. The calculated errors are the standard error.

Based on the above results, the binding affinities between the SARS-CoV-2 Mpro and the screened ligands were first predicted via Autodock Vina. The docking results revealed that the calculated binding free energies for all computed complexes varied from -2.4 to -9.2 kcal mol$^{-1}$. The average of binding free energies obtained of -5.99 kcal mol$^{-1}$ with the standard error of the mean of 1.08 kcal mol$^{-1}$. Based on the results, 27 top-lead ligands having the binding energy with SARS-CoV-2 Mpro more negative than -8.1 kcal mol$^{-1}$ (Table 2) were chosen to be further examined by the FPL simulations.

**Table 2**. Twenty-seven top-lead compounds obtained by docking and FPL simulations

| No | Name | ZINC ID | Affinity Energy | Average force (pN) | Average Work (kcal/mol) | Predicted $\Delta G^{Pre}_{FPL}$ |
|---|---|---|---|---|---|---|
| 1 | **Indocyanine green acid form** | **ZINC000008101127** | **-8.6** | **861.75 ± 42.65** | **94.55 ± 5.76** | **-10.81** |
| 2 | **Daclatasvir** | **ZINC000068204830** | **-8.1** | **590.59 ± 39.59** | **85.57 ± 6.52** | **-10.3** |
| 3 | **Teniposide** | **ZINC000004099009** | **-8.4** | **636.29 ± 28.39** | **71.74 ± 3.17** | **-9.53** |
| 4 | **Etoposide** | **ZINC000003938684** | **-8.1** | **652.51 ± 37.03** | **67.02 ± 4.55** | **-9.27** |
| 5 | **Levoleucovorin** | **ZINC000009212427** | **-8.1** | **610.87 ± 12.16** | **66.36 ± 1.89** | **-9.23** |
| 6 | **Naldemedine** | **ZINC000100378061** | **-8.2** | **648.26 ± 36.79** | **66.14 ± 3.12** | **-9.22** |
| 7 | **Cabozantinib** | **ZINC000070466416** | **-8.1** | **621.70 ± 28.96** | **62.88 ± 2.86** | **-9.03** |
| 8 | **Irinotecan** | **ZINC000001612996** | **-9** | **625.12 ± 41.31** | **62.15 ± 4.92** | **-8.99** |
| 9 | Azilsartan medoxomil | ZINC000014210642 | -8.2 | 550.68 ± 22.92 | 58.67 ± 3.46 | -8.8 |
| 10 | Ergotamine | ZINC000052955754 | -8.4 | 576.51 ± 25.68 | 58.63 ± 2.61 | -8.8 |

| | | | | | | |
|---|---|---|---|---|---|---|
| 11 | Cromolyn | ZINC000253632968 | -8.1 | 551.18 ± 37.07 | 55.90 ± 5.61 | -8.64 |
| 12 | Glecaprevir | ZINC000164528615 | -8.5 | 551.22 ± 40.48 | 55.54 ± 3.99 | -8.62 |
| 13 | Dolutegravir | ZINC000058581064 | -8.2 | 559.65 ± 24.05 | 55.05 ± 2.07 | -8.59 |
| 14 | Saquinavir | ZINC000029416466 | -8.1 | 514.50 ± 31.70 | 54.97 ± 5.12 | -8.59 |
| 15 | Dihydroergotamine | ZINC000003978005 | -8.7 | 543.99 ± 42.88 | 54.42 ± 5.10 | -8.56 |
| 16 | Accolate | ZINC000000896717 | -8.7 | 498.69 ± 32.54 | 52.91 ± 4.84 | -8.47 |
| 17 | Lumacaftor | ZINC000064033452 | -8.5 | 528.13 ± 36.91 | 50.37 ± 3.87 | -8.33 |
| 18 | Lifitegrast | ZINC000084668739 | -8.3 | 521.70 ± 22.03 | 49.47 ± 2.43 | -8.28 |
| 19 | Doxazosin | ZINC000094566092 | -8.1 | 524.16 ± 17.71 | 48.82 ± 2.18 | -8.25 |
| 20 | Rifaximin | ZINC000169621200 | -8.3 | 530.94 ± 42.43 | 45.23 ± 5.55 | -8.04 |
| 21 | Ceftaroline | ZINC000003989268 | -8.2 | 420.93 ± 53.33 | 44.59 ± 5.96 | -8.01 |
| 22 | Dutasteride | ZINC000003932831 | -8.1 | 499.62 ± 22.11 | 43.85 ± 2.42 | -7.97 |
| 23 | Imatinib | ZINC000019632618 | -8.3 | 474.81 ± 16.15 | 43.26 ± 3.02 | -7.93 |
| 24 | Raltegravir | ZINC000013831130 | -8.1 | 487.90 ± 22.66 | 43.05 ± 1.93 | -7.92 |
| 25 | Trypan blue | ZINC000169289767 | -9.2 | 409.97 ± 45.04 | 41.79 ± 7.06 | -7.85 |
| 26 | Nilotinib | ZINC000006716957 | -8.5 | 486.41 ± 26.65 | 39.98 ± 2.79 | -7.75 |
| 27 | Regorafenib | ZINC000006745272 | -8.3 | 425.92 ± 16.90 | 37.54 ± 2.99 | -7.61 |

## Docking binding pose

To investigate the binding interaction between the 27 top-lead compounds and SARS-CoV-2 Mpro, a detailed analysis of their possible docked conformation was performed to explore their interaction with the SARS-CoV-2 Mpro-binding pocket. Accordingly, the preferential binding pose of top-lead drugs obtained by docking simulations in the complex with SARS-CoV-2 Mpro was determined. The detailed interaction of SARS-CoV-2 Mpro and the full top-lead compounds are illustrated in Table S1. In particular, Figure 2 shows the particular binding of representative drugs including *daclatasvir, teniposide, etoposide*, and *levoleucovorin* with SARS-CoV-2 Mpro. Note that the substrate-binding site of SARS-CoV-2 Mpro resides in a cleft between domain I and domain II [10, 47]. The obtained results suggest that the top-lead drugs identified by the docking method bind to the substrate-binding cleft of SARS-CoV-2 Mpro via different hydrogen bonds (HBs). These compounds establish the sidechain interactions with a set of critical residues, including Thr26, His41, Leu141, Gly143, Ser144, Cys145, His163, Glu166, and Gln189, of SARS-CoV-2 Mpro. It should be noted that His41 and Cys145 reside in the Cys-His catalytic dyad and Glu166 is essential for dimerization of SARS-CoV-2 Mpro [7, 10].

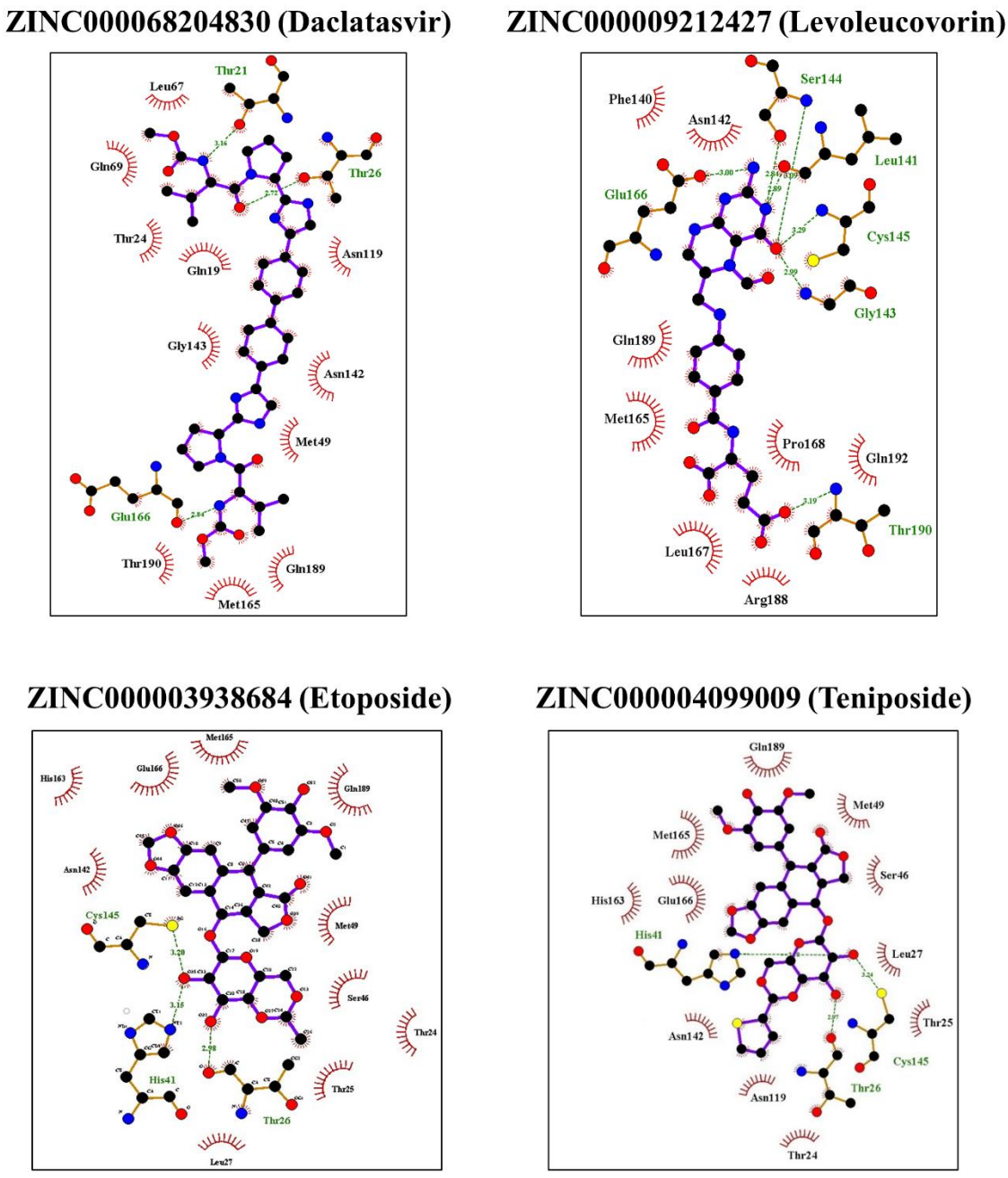


**Figure 2**. The detailed interactions between SARS-CoV-2 Mpro and four drugs obtained via molecular docking simulations are illustrated by the LigPlot$^{++}$ program [44]. Residues of SARS-CoV-2 Mpro forming HBs and sidechain interactions with ligands are indicated in green and black, respectively. Atoms of carbon, oxygen, nitrogen, and sulfur are presented in black, red, blue, and yellow, respectively.

## FPL simulation

The molecular docking simulations were performed with numerous limitations such as inflexible receptor and small number trial positions of inhibitors, the MD/SMD simulations were thus executed to refine the outcomes [48, 49]. In this context, the FPL simulations were manipulated to re-rank the ligand-binding affinity to the SARS-CoV-2 Mpro since the approach successfully formed an appropriate outcome compared with the respective experiments, $R = 0.76$ [13]. During MD/SMD calculations, the complexes were first relaxed to the equilibrated states. The clustering method was then employed to estimate the stabilized structures of the complexes of SARS-CoV-2 Mpro and ligands with an all-atom root-mean-square deviation (RMSD) cutoff of 3.0 Å. The dominant conformations of the top-lead compounds in the complex with SARS-CoV-2 Mpro are depicted in Table S2. Since changing from the implicit solvent environment (docking results) to the explicit solvent modeling (MD simulations), the complex structures were slightly refined with an averaged RMSD between the initial and MD refine of ligands of ca. 2.0 Å. The structural changes of representative compounds are described in Figure 3. Although the value of RMSD is small, implying the success of the docking calculation, some charged groups of the ligands were also rotated and then formed HBs to the receptor. The shifts are small but important, resulting in the difference of the affinity ranking order of ligands (cf. Table 2).

Over the FPL simulations, the maximal value of external force called rupture force and the pulling work averaged from 8 independent SMD simulation trajectories were both used as criteria to rank the ligand affinity. However, the pulling work is more appropriate than the rupture force because it directly associates with the ligand-binding free energy via isobaric−isothermal Jarzynski's equality [22]. The average of pulling forces of all complexes between SARS-CoV-2 and tested ligands in a time-dependent manner is shown in Table S3. The obtained results indicated that the mean rupture forces ranged from 409.97 ± 45.04 (*trypan blue free acid*) to 861.75 ± 42.65 (*indocyanine green acid form*) pN with the average value of 552 ± 31.4 pN (Table 2). The pulling work was shown to be a key factor representing the binding of ligands and the protein [22, 23]. According to FPL calculations, the average pulling works of the tested 27 compounds fell within a

range of 37.54 ± 2.99 (*regorafenib*) to 94.55 ± 5.76 (*indocyanine green acid form*) kcal•mol$^{-1}$ with the mean value of 55.94 ± 3.02 kcal•mol$^{-1}$ (Table 2).

Every complex of SARS-CoV-2 Mpro and ligand was computed over 8 independent FPL simulations which initiated from the same conformation but different in random velocity. One FPL trajectory consists of 0.1 ns of NVT, 2.0 ns of NPT, and 0.5 ns of SMD simulations. Totally, 20.8 ns of MD simulations were computed to evaluate the ligand-binding affinity with SARS-CoV-2 Mpro. The binding affinity of a ligand to the SARS-CoV-2 Mpro can thus be simulated 8 times during approximately 6 hours. Consequently, without the requirement of a professional computing system, the low CPU consumption allows the precise evaluation of the binding affinity of various compounds with SARS-CoV-2 Mpro at an appropriate time.

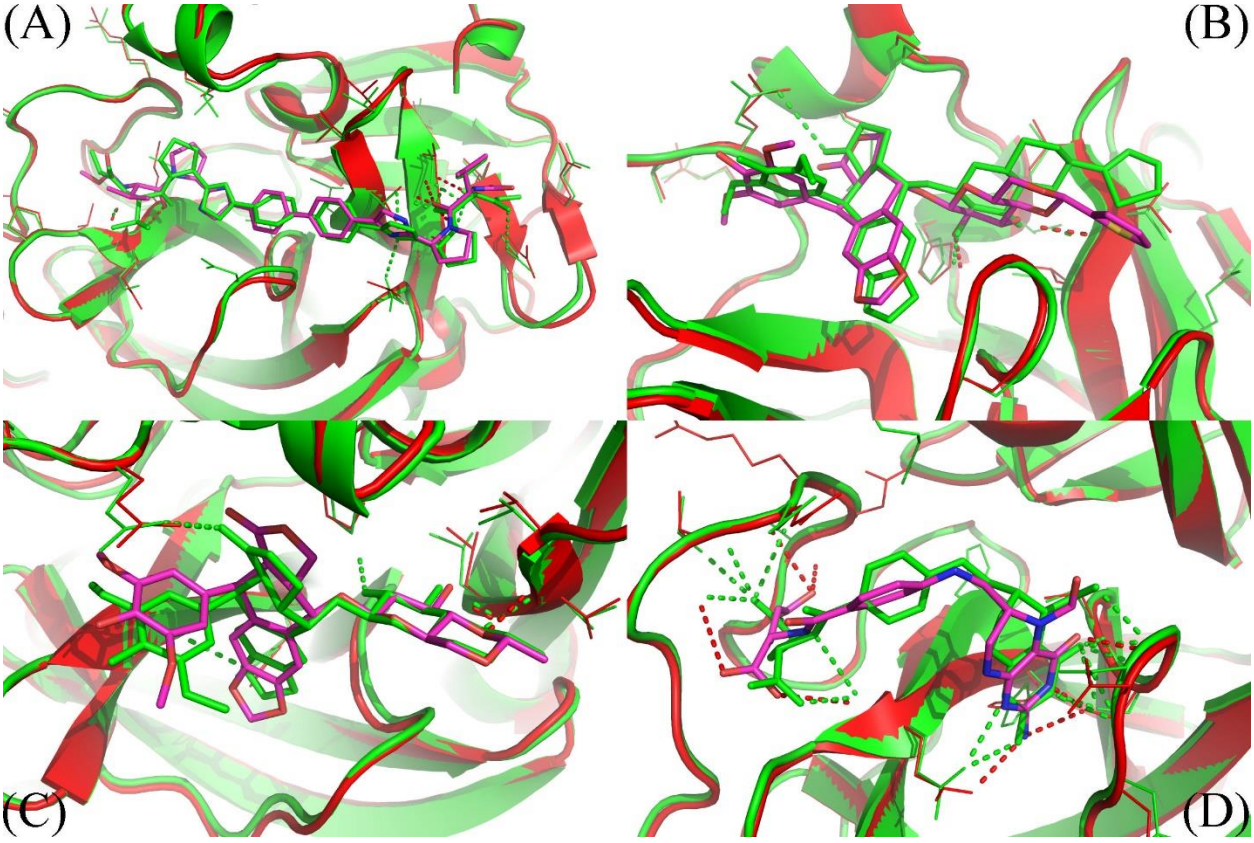


**Figure 3**. The comparison between MD refined conformations of the complexes and docked structures. The MD refined structure was obtained by all-atom clustering with a cut-off of 0.3 nm over the last NPT snapshots. (A) is the *daclatasvir* complex; (B) is the

*teniposide* system; (C) is the *etoposide* complex; (D) is the *levoleucovorin* system. Both receptors and ligands obtained from docking are displayed in green.

Recently, the FPL calculations have been proved to adopt a good agreement with the experimental data for SARS-CoV-2 Mpro and its inhibitors [12, 13, 41]. The estimated binding free energies $\Delta G_{\mathrm{FPL}}^{\mathrm{Pre}}$ between top-lead ligands and SARS-CoV-2 Mpro were thus calculated in the same way as in the previous study [13]. The obtained results are shown in Table 2. The ligand with the predicted $\Delta G_{\mathrm{FPL}}^{\mathrm{Pre}}$ more negative than -9.0 kcal•mol$^{-1}$ is thus strongly expected to be capable of inhibiting the function of the SARS-CoV-2 Mpro protein. Noted that *indocyanine green acid form* is a fluorescent dye used in medical diagnostics as an indicator substance in cardiac, circulatory, hepatic, and ophthalmic conditions [50] which might not be suitable to serve as a drug for COVID-19 treatment. Consequently, seven approved drugs including *daclatasvir, teniposide, etoposide, levoleucovorin, naldemedine*, *cabozantinib,* and *irinotecan* were predicted as the very promising inhibitors of SARS-CoV-2 Mpro in practice due to their high binding affinities calculated (Table 2).

## The most potential inhibitors of SARS-CoV-2 Mpro identified

The 2D structures of 7 top-lead ligands of SARS-CoV-2 Mpro ranked by the FPL simulations are illustrated in Figure 4. Except for *levoleucovorin* and *cabozantinib* of which molecular structures are considered as flexible, the other 5 compounds possess the rigid structure and thus, lacking molecular flexibility. However, the substrate-binding cleft on the surface of SARS-CoV-2 Mpro is expected to be flexible to sizably accommodate a broad type of compound [14]. Importantly, all of the 7 top-lead inhibitors predicted have many sites to form intermolecular HBs with the protein, hence being able to strongly interact with SARS-CoV-2 Mpro.

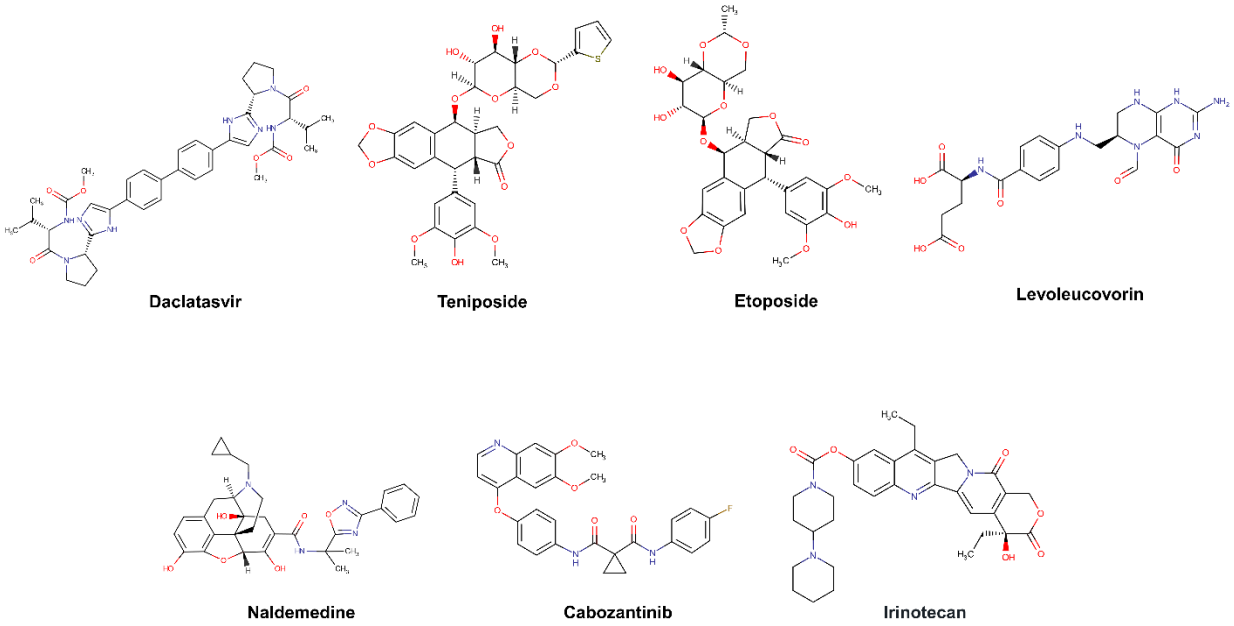


**Figure 4**. 2D structure of potential inhibitors for SARS-CoV-2 Mpro predicted by molecular docking and FPL simulations from the ZINC15 sub-database named FDA-approved drugs.

*Daclatasvir* belonging to a valine and derivatives group is a direct-acting antiviral agent against Hepatitis C Virus (HCV), a positive-sense single-stranded RNA virus [51]. Previously, the anti-HCV drug was shown to be effective in the treatment of Middle East Respiratory Syndrome (MERS) coronavirus [52]. Therefore, anti-HCV drugs are expected to express a common antiviral activity against human coronaviruses. From our calculation, *daclatasvir* showed the highest affinity to SARS-CoV-2 Mpro among tested compounds (cf. Table 2) via forming HBs with a critical residue Glu166 and other residues, namely Thr21 and Thr26 (Figure 2). Notably, it was shown that the combined use of *sofosbuvir* and *daclatasvir* improved the survival and clinical recovery of COVID-19 patients with modest to intense symptoms [53]. The introduction of *sofosbuvir* and *daclatasvir* to standard care could reduce the hospitalization time for COVID-19 patients in comparison to standard care alone [54, 55]. These results indicated that *daclatasvir* is very promising in the treatment of COVID-19 patients and that our approach successfully selected the practically potential drug for COVID-19 therapy.

It is believed that both virus-infected and cancer cells require the elevation of nucleic acids and protein synthesis and energy metabolism. Thus, drugs inhibiting cancer cells can be effective in the suppression of viral replication. Indeed, different antineoplastic agents re-purposed for COVID-19 therapy have been applied for early clinical trials [56, 57]. *Etoposide* and *teniposide* are anticancer drugs for the treatment of several types of tumors, leukemia, and lymphoma [58]. *Etoposide* and *teniposide* are both semisynthetic analogs of podophyllotoxin. They share a similar basic structure of the parent podophyllotoxin while the carbohydrate moiety of a methyl group in *etoposide* is substituted for a thenylidene group in *teniposide* [58], inducing a slight difference in binding affinities to SARS-CoV-2 Mpro (cf. Table 2). These two compounds are estimated to establish HBs with key residues Cy145 and His41 and residue Thr26 (Figure 2). *Teniposide* possesses a logP value of 2.78 (DrugBank, Accession Number DB00444) while *etoposide* has a lower logP value of 1.16 (DrugBank, Accession Number DB00773). These values are in the optimal range of 1 to 3 for a compound to achieve appropriate physicochemical characteristics [59]. However, *teniposide* which is predicted to have a higher affinity to SARS-CoV-2 Mpro has better membrane permeability. *Irinotecan* is indicated for colorectal and pancreatic cancer treatment or combined with *cisplatin* for the cure of small cell lung cancer [60-62]. The Sn38 moiety is believed to mainly impact the high binding affinity of *irinotecan* to SARS-CoV-2 Mpro [14]. The compound is predicted to form HBs with residues Thr24 and Thr26 of SARS-CoV-2 Mpro (Table S1). *Irinotecan* (DrugBank, Accession Number DB00762) has a similar logP value and molecular weight to *teniposide*, indicating a comparable membrane permeability. In general, these three anti-cancer drugs are highly promising in the treatment of COVID-19.

*Levoleucovorin*, a folate analog, is utilized in rescue therapy to recover cells from the toxic effects of folate antagonists such as methotrexate after high-dose treatment in osteosarcoma therapy [63]. *Naldemedine* is an opioid receptor antagonist and used for the treatment of opioid-induced constipation [64]. *Levoleucovorin* and *naldemedine* share similar estimated binding affinities to SARS-CoV-2 Mpro (cf. Table 2). While *naldemedine* is predicted to form HBs with residues Thr24 and Ser46 (Table S1), *levoleucovorin* is expected to establish several HBs with both critical residues Cys145 and Glu166 and other residues including Leu141, Gly143, Ser144, and Thr190 (Figure 2). Nevertheless,

*levoleucovorin* is hydrophilic with a low logP value of -2.8 (DrugBank, Accession Number DB11596), pointing out that the compound is not suitable as a drug for COVID-19 treatment. Meanwhile, *naldemedine* shows a logP value of 2.43, indicating its good ability to be transported through a cellular membrane.

*Cabozantinib* suppresses metastasis and oncogenesis by inhibiting receptor tyrosine kinases [65]. Recently, several kinase inhibitors have been re-purposed for COVID-19 therapy [66, 67]. The molecular structure of *cabozantinib* is not too bulky, flexible, and contains Fluoro, an element that can be found in many bioactive compounds. *Cabozantinib* is predicted to establish HBs with residues Ser46, Gly143 and a key residue Glu166 of SARS-CoV-2 Mpro (Table S1). The high logP value 4.66 of *cabozantinib* (DrugBank, Accession Number DB08875) indicating the considerable level of toxicity may limit the application of this drug in practical use.

## Conclusion

Since the COVID-19 pandemic spread throughout the world, several inhibitors of SARS-CoV-2 Mpro have been identified experimentally [10, 68]. Based on CADD, various computational studies have also been conducted to search for the promising inhibitors of Mpro and other critical enzymes of SARS-CoV-2 [12, 13, 69-71]. Previously, a combination of molecular docking and FPL simulations was proved to efficiently predict the binding affinity of a ligand to SARS-CoV-2 Mpro. In this study, the same approach was employed to estimate the promising inhibitors for SARS-CoV-2 Mpro from a set of 2100 FDA-approved drugs. The binding conformation of the top-lead compounds identified with SARS-CoV-2 Mpro was also analyzed. The detailed interactions of the seven top-lead drugs including *daclatasvir, teniposide, etoposide, levoleucovorin, naldemedine*, *cabozantinib,* and *irinotecan* that have the predicted binding free energies with SARS-CoV-2 Mpro less than -9.00 kcal•mol$^{-1}$ indicated that these drugs all occupied the substrate-binding pocket of SARS-CoV-2 Mpro and thus potentially hindered the protease activity of the enzyme. These drugs interact with important residues of SARS-CoV-2 Mpro including Thr26, His41, Leu141, Gly143, Ser144, Cys145, His163, Glu166, and Gln189. Further *in vitro* and *in vivo* investigations are needed to be performed to validate the obtained results.

## Declaration of competing interest

The authors declared that they have no conflicts of interest to this work.

## Data availability statement

The authors confirm that the data supporting the findings of this study are available within the article and its supplementary materials.

## Acknowledgements

This work was supported by Vietnam National Foundation for Science & Technology Development (NAFOSTED).

## Reference

[1] Cucinotta, D., Vanelli, M. WHO declares COVID-19 a pandemic. Acta bio-medica: Atenei Parmensis. 2020, 91, 157-60.
[2] Li, Q., Guan, X., Wu, P., Wang, X., Zhou, L., Tong, Y., et al. Early transmission dynamics in Wuhan, China, of novel coronavirus–infected pneumonia. New England Journal of Medicine. 2020.
[3] Mizumoto, K., Chowell, G. Estimating the risk of 2019 novel coronavirus death during the course of the outbreak in China, 2020. medRxiv. 2020.
[4] Worldometers. COVID-19 CORONAVIRUS PANDEMIC. 2020, Vol. 2021.
[5] He, F., Deng, Y., Li, W. Coronavirus disease 2019: What we know? Journal of medical virology. 2020, 92, 719-25.
[6] Naqvi, A.A.T., Fatima, K., Mohammad, T., Fatima, U., Singh, I.K., Singh, A., et al. Insights into SARS-CoV-2 genome, structure, evolution, pathogenesis and therapies: Structural genomics approach. Biochimica et Biophysica Acta (BBA)-Molecular Basis of Disease. 2020, 165878.
[7] Jin, Z., Du, X., Xu, Y., Deng, Y., Liu, M., Zhao, Y., et al. Structure of M pro from SARS-CoV-2 and discovery of its inhibitors. Nature. 2020, 1-5.
[8] Olubiyi, O.O., Olagunju, M., Keutmann, M., Loschwitz, J., Strodel, B. High throughput virtual screening to discover inhibitors of the main protease of the coronavirus SARS-CoV-2. Molecules. 2020, 25, 3193.
[9] Pillaiyar, T., Manickam, M., Namasivayam, V., Hayashi, Y., Jung, S.-H. An overview of severe acute respiratory syndrome–coronavirus (SARS-CoV) 3CL protease inhibitors: peptidomimetics and small molecule chemotherapy. Journal of medicinal chemistry. 2016, 59, 6595-628.
[10] Zhang, L., Lin, D., Sun, X., Curth, U., Drosten, C., Sauerhering, L., et al. Crystal structure of SARS-CoV-2 main protease provides a basis for design of improved α-ketoamide inhibitors. Science. 2020, 368, 409-12.

[11] Dai, W., Zhang, B., Jiang, X.-M., Su, H., Li, J., Zhao, Y., et al. Structure-based design of antiviral drug candidates targeting the SARS-CoV-2 main protease. Science. 2020, 368, 1331-5.
[12] Ngo, S.T., Quynh Anh Pham, N., Thi Le, L., Pham, D.-H., Vu, V.V. Computational determination of potential inhibitors of SARS-CoV-2 main protease. Journal of chemical information and modeling. 2020.
[13] Pham, M.Q., Vu, K.B., Pham, T.N.H., Tran, L.H., Tung, N.T., Vu, V.V., et al. Rapid prediction of possible inhibitors for SARS-CoV-2 main protease using docking and FPL simulations. RSC Advances. 2020, 10, 31991-6.
[14] Ngo, S.T., Hung Minh, N., Le Thi Thuy, H., Pham Minh, Q., Vi Khanh, T., Nguyen Thanh, T., et al. Assessing Potential Inhibitors for SARS-CoV-2 Main Protease from Available Drugs using Free Energy Perturbation Simulations. RSC Adv. 2020, 10, 40284-90.
[15] Pham, M.Q., Vu, K.B., Han Pham, T.N., Thuy Huong, L.T., Tran, L.H., Tung, N.T., et al. Rapid prediction of possible inhibitors for SARS-CoV-2 main protease using docking and FPL simulations. RSC Adv. 2020, 10, 31991-6.
[16] Yu, W., MacKerell, A.D., Jr. Computer-Aided Drug Design Methods. Methods in molecular biology. 2017, 1520, 85-106.
[17] Marshall, G.R. Computer-aided drug design. Annual review of pharmacology and toxicology. 1987, 27, 193-213.
[18] Ngo, S.T., Nguyen, T.H., Tung, N.T., Nam, P.C., Vu, K.B., Vu, V.V. Oversampling Free Energy Perturbation Simulation in Determination of the Ligand-Binding Free Energy. J. Comput. Chem. 2020, 41, 611-8.
[19] Homeyer, N., Stoll, F., Hillisch, A., Gohlke, H. Binding Free Energy Calculations for Lead Optimization: Assessment of Their Accuracy in an Industrial Drug Design Context. Journal of Chemical Theory and Computation. 2014, 10, 3331-44.
[20] Ngo, S.T., Vu, K.B., Bui, L.M., Vu, V.V. Effective Estimation of Ligand-Binding Affinity Using Biased Sampling Method. ACS Omega. 2019, 4, 3887-93.
[21] Ngo, S.T. Estimating the ligand-binding affinity via λ-dependent umbrella sampling simulations. J. Comput Chem. 2021, 42, 117-23.
[22] Ngo, S.T., Hung, H.M., Nguyen, M.T. Fast and accurate determination of the relative binding affinities of small compounds to HIV-1 protease using non-equilibrium work. Journal of Computational Chemistry. 2016, 37, 2734-42.
[23] Mai, N.T., Lan, N.T., Vu, T.Y., Duong, P.T.M., Tung, N.T., Phung, H.T.T. Estimation of the ligand-binding free energy of checkpoint kinase 1 via non-equilibrium MD simulations. Journal of Molecular Graphics and Modelling. 2020, 100, 107648.
[24] Tam, N.M., Nam, P.C., Quang, D.T., Tung, N.T., Vu, V.V., Ngo, S.T. Binding of Inhibitors to the Monomeric and Dimeric SARS-CoV-2 Mpro. RSC Adv. 2021, 11, 2926-34.
[25] Sterling, T., Irwin, J.J. ZINC 15--Ligand Discovery for Everyone. J. Chem. Inf. Model. 2015, 55, 2324-37.
[26] Trott, O., Olson, A.J. AutoDock Vina: improving the speed and accuracy of docking with a new scoring function, efficient optimization, and multithreading. Journal of computational chemistry. 2010, 31, 455-61.

[27] Morris, G.M., Huey, R., Lindstrom, W., Sanner, M.F., Belew, R.K., Goodsell, D.S., et al. AutoDock4 and AutoDockTools4: Automated docking with selective receptor flexibility. Journal of computational chemistry. 2009, 30, 2785-91.
[28] Nguyen, N.T., Nguyen, T.H., Pham, T.N.H., Huy, N.T., Bay, M.V., Pham, M.Q., et al. Autodock Vina Adopts More Accurate Binding Poses but Autodock4 Forms Better Binding Affinity. Journal of Chemical Information and Modeling. 2019, 60, 204-11.
[29] Gasteiger, J., Marsili, M. A new model for calculating atomic charges in molecules. Tetrahedron Letters. 1978, 19, 3181-4.
[30] Gasteiger, J., Marsili, M. Iterative partial equalization of orbital electronegativity—a rapid access to atomic charges. Tetrahedron. 1980, 36, 3219-28.
[31] Forli, S., Huey, R., Pique, M.E., Sanner, M.F., Goodsell, D.S., Olson, A.J. Computational protein–ligand docking and virtual drug screening with the AutoDock suite. Nature protocols. 2016, 11, 905-19.
[32] Abraham, M.J., Murtola, T., Schulz, R., Páll, S., Smith, J.C., Hess, B., et al. GROMACS: High performance molecular simulations through multi-level parallelism from laptops to supercomputers. SoftwareX. 2015, 1, 19-25.
[33] Aliev, A.E., Kulke, M., Khaneja, H.S., Chudasama, V., Sheppard, T.D., Lanigan, R.M. Motional timescale predictions by molecular dynamics simulations: case study using proline and hydroxyproline sidechain dynamics. Proteins: Structure, Function, and Bioinformatics. 2014, 82, 195-215.
[34] Jorgensen, W.L., Chandrasekhar, J., Madura, J.D., Impey, R.W., Klein, M.L. Comparison of simple potential functions for simulating liquid water. The Journal of chemical physics. 1983, 79, 926-35.
[35] Wang, J., Wang, W., Kollman, P.A., Case, D.A. Automatic atom type and bond type perception in molecular mechanical calculations. Journal of molecular graphics and modelling. 2006, 25, 247-60.
[36] Case, D.A., Ben-Shalom, I.Y., Brozell, S.R., Cerutti, D.S., Cheatham, T.E.C., III, V.W.D. , Darden, T.A., et al. AMBER 18. University of California, San Francisco. 2018.
[37] Zhang, H., Yin, C., Jiang, Y., van der Spoel, D. Force Field Benchmark of Amino Acids: I. Hydration and Diffusion in Different Water Models. J. Chem. Inf. Model. 2018, 58, 1037-52.
[38] Zhang, H., Jiang, Y., Cui, Z., Yin, C. Force Field Benchmark of Amino Acids. 2. Partition Coefficients between Water and Organic Solvents. J. Chem. Inf. Model. 2018, 58, 1669-81.
[39] Wang, J., Wolf, R.M., Caldwell, J.W., Kollman, P.A., Case, D.A. Development and testing of a general amber force field. Journal of computational chemistry. 2004, 25, 1157-74.
[40] Da Silva, A.W.S., Vranken, W.F. ACPYPE-Antechamber python parser interface. BMC research notes. 2012, 5, 367.
[41] Ngo, S.T., Tam, N.M., Pham, M.Q., Nguyen, T.H. A Benchmark of Popular Free Energy Approaches Revealing the Inhibitors Binding to SARS-CoV2 Mpro. 2020.
[42] Ngo, S.T., Hung, H.M., Nguyen, M.T. Fast and Accurate Determination of the Relative Binding Affinities of Small Compounds to HIV-1 Protease using Non-Equilibrium Work. J. Comput. Chem. 2016, 37, 2734-42.

[43] Ngo, S.T., Nguyen, M.T., Nguyen, M.T. Determination of the absolute binding free energies of HIV-1 protease inhibitors using non-equilibrium molecular dynamics simulations. Chem. Phys. Lett. 2017, 676, 12-7.
[44] Laskowski, R.A., Swindells, M.B. LigPlot+: multiple ligand–protein interaction diagrams for drug discovery. ACS Publications, 2011.
[45] Trott, O., Olson, A.J. AutoDock Vina: improving the speed and accuracy of docking with a new scoring function, efficient optimization, and multithreading. J Comput Chem. 2010, 31, 455-61.
[46] Amin, S.A., Banerjee, S., Ghosh, K., Gayen, S., Jha, T. Protease targeted COVID-19 drug discovery and its challenges: Insight into viral main protease (Mpro) and papain-like protease (PLpro) inhibitors. Bioorganic & Medicinal Chemistry. 2020, 115860.
[47] Anand, K., Palm, G.J., Mesters, J.R., Siddell, S.G., Ziebuhr, J., Hilgenfeld, R. Structure of coronavirus main proteinase reveals combination of a chymotrypsin fold with an extra α-helical domain. EMBO J. 2002, 21, 3213-24.
[48] Decherchi, S., Cavalli, A. Thermodynamics and Kinetics of Drug-Target Binding by Molecular Simulation. Chem. Rev. 2020.
[49] Genheden, S., Ryde, U. The MM/PBSA and MM/GBSA Methods to Estimate Ligand-Binding Affinities. Expert Opin. Drug Discov. 2015, 10, 449-61.
[50] Alander, J.T., Kaartinen, I., Laakso, A., Pätilä, T., Spillmann, T., Tuchin, V.V., et al. A review of indocyanine green fluorescent imaging in surgery. International journal of biomedical imaging. 2012, 2012.
[51] Smith, M.A., Regal, R.E., Mohammad, R.A. Daclatasvir: A NS5A replication complex inhibitor for hepatitis C infection. Annals of Pharmacotherapy. 2016, 50, 39-46.
[52] Elfiky, A.A., Mahdy, S.M., Elshemey, W.M. Quantitative structure-activity relationship and molecular docking revealed a potency of anti-hepatitis C virus drugs against human corona viruses. Journal of medical virology. 2017, 89, 1040-7.
[53] Simmons, B., Wentzel, H., Mobarak, S., Eslami, G., Sadeghi, A., Asgari, A.A., et al. Sofosbuvir/daclatasvir regimens for the treatment of COVID-19: an individual patient data meta-analysis. Journal of Antimicrobial Chemotherapy. 2020.
[54] Eslami, G., Mousaviasl, S., Radmanesh, E., Jelvay, S., Bitaraf, S., Simmons, B., et al. The impact of sofosbuvir/daclatasvir or ribavirin in patients with severe COVID-19. Journal of Antimicrobial Chemotherapy. 2020, 75, 3366-72.
[55] Sadeghi, A., Ali Asgari, A., Norouzi, A., Kheiri, Z., Anushirvani, A., Montazeri, M., et al. Sofosbuvir and daclatasvir compared with standard of care in the treatment of patients admitted to hospital with moderate or severe coronavirus infection (COVID-19): a randomized controlled trial. Journal of Antimicrobial Chemotherapy. 2020, 75, 3379-85.
[56] Ciliberto, G., Mancini, R., Paggi, M.G. Drug repurposing against COVID-19: focus on anticancer agents. Journal of Experimental & Clinical Cancer Research. 2020, 39, 1-9.
[57] El Bairi, K., Trapani, D., Petrillo, A., Le Page, C., Zbakh, H., Daniele, B., et al. Repurposing anticancer drugs for the management of COVID-19. European Journal of Cancer. 2020.
[58] Clark, P.I., Slevin, M.L. The clinical pharmacology of etoposide and teniposide. Clinical pharmacokinetics. 1987, 12, 223-52.
[59] Arnott, J.A., Planey, S.L. The influence of lipophilicity in drug discovery and design. Expert opinion on drug discovery. 2012, 7, 863-75.

[60] Ramesh, M., Ahlawat, P., Srinivas, N.R. Irinotecan and its active metabolite, SN-38: review of bioanalytical methods and recent update from clinical pharmacology perspectives. Biomedical chromatography. 2010, 24, 104-23.
[61] Noda, K., Nishiwaki, Y., Kawahara, M., Negoro, S., Sugiura, T., Yokoyama, A., et al. Irinotecan plus cisplatin compared with etoposide plus cisplatin for extensive small-cell lung cancer. New England Journal of Medicine. 2002, 346, 85-91.
[62] Rahman, F.A.u., Ali, S., Saif, M.W. Update on the role of nanoliposomal irinotecan in the treatment of metastatic pancreatic cancer. Therapeutic advances in gastroenterology. 2017, 10, 563-72.
[63] Chuang, V.T.G., Suno, M. Levoleucovorin as replacement for leucovorin in cancer treatment. Annals of Pharmacotherapy. 2012, 46, 1349-57.
[64] Blair, H.A. Naldemedine: a review in opioid-induced constipation. Drugs. 2019, 79, 1241-7.
[65] Grüllich, C. Cabozantinib: a MET, RET, and VEGFR2 tyrosine kinase inhibitor. In: Small Molecules in Oncology, Springer, 2014, pp. 207-14.
[66] Weisberg, E., Parent, A., Yang, P.L., Sattler, M., Liu, Q., Liu, Q., et al. Repurposing of kinase inhibitors for treatment of COVID-19. Pharmaceutical research. 2020, 37, 1-29.
[67] Weston, S., Coleman, C.M., Sisk, J.M., Haupt, R., Logue, J., Matthews, K., et al. Broad anti-coronaviral activity of FDA approved drugs against SARS-CoV-2 in vitro and SARS-CoV in vivo. bioRxiv. 2020.
[68] Mohammad, T., Shamsi, A., Anwar, S., Umair, M., Hussain, A., Rehman, M.T., et al. Identification of high-affinity inhibitors of SARS-CoV-2 main protease: Towards the development of effective COVID-19 therapy. Virus research. 2020, 288, 198102.
[69] Romeo, A., Iacovelli, F., Falconi, M. Targeting the SARS-CoV-2 spike glycoprotein prefusion conformation: virtual screening and molecular dynamics simulations applied to the identification of potential fusion inhibitors. Virus research. 2020, 286, 198068.
[70] Bhowmik, D., Nandi, R., Jagadeesan, R., Kumar, N., Prakash, A., Kumar, D. Identification of potential inhibitors against SARS-CoV-2 by targeting proteins responsible for envelope formation and virion assembly using docking based virtual screening, and pharmacokinetics approaches. Infection, Genetics and Evolution. 2020, 84, 104451.
[71] Dey, D., Borkotoky, S., Banerjee, M. In silico identification of Tretinoin as a SARS-CoV-2 envelope (E) protein ion channel inhibitor. Computers in biology and medicine. 2020, 104063.